Back-side-coated chirped mirrors with ultra-smooth broadband dispersion characteristics

N. Matuschek, L. Gallmann, D.H. Sutter, G. Steinmeyer, U. Keller

Ultrafast Laser Physics Laboratory, Institute of Quantum Electronics, Swiss Federal Institute of Technology, ETH Hönggerberg − HPT,
8093 Zürich, Switzerland
(Fax: +41-1/633-1059, E-mail: sguenter@iqe.phys.ethz.ch)

Abstract. We demonstrate a new technique for the design of chirped mirrors with extremely smooth dispersion characteristics over an extended ultra-broadband wavelength range. Our approach suppresses spectral dispersion oscillations, which can lead to unwanted strong spectral modulations and limit the bandwidth of mode-locked laser pulses. Dispersion oscillations are significantly reduced by coating the chirped mirror structure on the back side of a substrate, providing ideal impedance matching between coating and ambient medium. An anti-reflection coating may be added on the front side of the substrate, geometrically separated from the chirped mirror. The chirped mirror structure and the anti-reflection coating are non-interfering and can be independently designed and optimized. The separation of both coating sections provides a much better solution for the impedance-matching problems than previous approaches to chirped mirror design. We show by a theoretical analysis and numerical simulations that minimum dispersion oscillations are achieved if the index of the substrate is identical to the index of one of the coating materials and if double-chirping is used for the chirped mirror structure. Based on this analysis, we design a mirror that supports a bandwidth of 220 THz with group delay dispersion oscillations of about $2\,\mathrm{fs}^2$ (rms), an order-of magnitude improvement compared to previous designs of similar bandwidth. In a first experimental demonstration of back-side-coated (BASIC) mirrors, we achieve nearly transform-limited and virtually unchirped pulses of 5.8 fs duration from a Kerr-lens mode-locked Ti:sapphire laser. BASIC mirrors are particularly suited for higher-order dispersion compensation schemes. They support the extremely broad spectra of few-cycle pulses and promise to provide clean pulse shapes in this regime.

PACS: 42.65.Re; 42.79.Bh; 42.79.Wc

Over the last few years, ultra short-pulse generation in the sub-10-fs regime has advanced at a rapid pace, leading to sub-6-fs pulses directly from a laser oscillator [1, 2]. Retracing the history of ultra fast oscillators, it becomes clear that several major steps towards shorter pulse duration have been enabled by improved dispersion-compensation schemes. The long-standing world record of 6-fs pulse duration was achieved by optimized third-order dispersion in the pulse compressor [3]. The first sub-10-fs laser pulses directly from a Ti:sapphire laser were obtained by using silver mirrors as high reflectors and a prism pair for dispersion compensation [4]. This laser was operated at a wavelength where the prism pair provides simultaneous second- and third-order dispersion compensation. However, considerable residual higher-order contributions prevented this laser from producing pulses shorter than ≈ 8.5 fs. The invention of chirped mirrors by Szipöcs et al. set a new milestone in ultra short-pulse generation [5]. Today, ultra short-pulse generation in the 5-fs regime generally relies on chirped mirrors. Chirped mirrors are used in Ti:sapphire lasers, external compression schemes [6, 7], and optical parametric amplification [8]. Ultimately, chirped mirrors do not support an unrestricted bandwidth and limit further pulse shortening [9]. Thus, further improvements in chirped mirror design and fabrication are mandatory for the generation of shorter pulses.

The basic idea behind a chirped mirror is relatively simple: layers with increasing thickness (e.g., quarter-wave layers with a gradually increasing Bragg wavelength) are stacked such that longer wavelengths penetrate deeper into the mirror structure, producing a negative group-delay dispersion (GDD). More precisely, the GDD of a chirped mirror is designed such that the dispersion of other elements in the laser cavity is compensated for. Additionally, these mirrors provide an enhanced high-reflectance bandwidth compared to standard dielectric quarter-wave mirrors. In combination, this allows for a more efficient compensation of higher-order dispersion over a broader spectral range than prisms do. In [10] ≈ 7.5-fs pulses were reported for a prism-less ring oscillator using only chirped mirrors, which provided dispersion compensation over a bandwidth $\Delta \nu \approx 85$ THz (710–890 nm).

However, chirped mirrors have one important drawback. The designed mirror dispersion shows unwanted spectral oscillations around the target function. These oscillations are caused by an impedance mismatch of the chirped mirror

structure to the ambient medium, which is typically air [11]. Generally, the amplitude of dispersion oscillations dramatically increases with mirror bandwidth. A powerful approach to address this problem of mirror design is the concept of double-chirped mirrors (DCMs, [12]). In a DCM the different matching problems are solved by different multilayer subsections [13] (see Fig. 1a). The technique of double-chirping matches the impedance of the chirped mirror section to the low-index or high-index material of the coating, which is then matched to ambient air by an additional anti-reflection (AR) coating on top of the chirped mirror.

With one of our first sets of DCMs we readily generated pulses of 6.5-fs duration [14]. Dispersion compensation was obtained over a bandwidth of $\Delta\nu \approx 115$ THz (680–920 nm). Further improvements in both the theoretical understanding of a DCM [13] and in the layer-deposition accuracy finally resulted in pulses in the two-optical-cycle regime. The dispersion-compensation bandwidth supported by the DCMs used in these lasers is $\Delta\nu \approx 180$ THz [1]. Inevitable imperfections of the AR coating, which provides the impedance-matching step to air, are the limiting factor in such ultra-broadband designs. Consequently, the enormous bandwidth can only be supported with an additional cancellation of dispersion oscillations. This cancellation is achieved by using combinations of DCMs under different angles of incidence [1, 15]. Alternatively, suitably designed combinations of mirrors from different coating runs may be used [16].

Because of the limiting trade-off boundary condition between dispersion-oscillation amplitude and bandwidth, further improvement of pulse bandwidth with conventional chirped mirrors appears to be difficult. In this paper, we present a novel chirped mirror concept, which suppresses detrimental dispersion oscillations by design. This is achieved by geometrically separating the chirped mirror stack from the AR section, coating them on two non-interfering surfaces of

a substrate. As illustrated in Fig. 1b, the AR coating is coated on the front side and the chirped mirror on the back side of the substrate. Therefore, we call these mirrors back-side-coated (BASIC) mirrors. This approach provides a better solution to impedance-matching problems in chirped mirror design. The refractive index of the substrate can be chosen close to the refractive index of the low-index coating material. This avoids the discontinuity of the refractive index at the interface to air. In such a situation, dispersion oscillations can be almost completely removed [17]. Other than standard DCMs, BASIC mirrors do not require the front AR coating for a reduction of dispersion oscillations. A nearly total elimination of dispersion oscillations is achieved by non-interfering front and back surfaces. For the BASIC mirror, the AR is merely required to avoid additional losses, i.e., to increase the net reflectance of the mirror. Consequently, the BASIC technique allows compensation for the dispersion over a much broader bandwidth with strongly reduced dispersion oscillations. As a consequence of the passage through bulk material, the additional positive material dispersion reduces the achievable negative net GDD of such a mirror. Hence, the most powerful applications of BASIC mirrors are combinations with other dispersion-compensating elements like grating or prism sequences, which allow for a pre-compensation of second-order dispersion. BASIC mirrors can then be used to correct higher-order dispersion.

This paper widely uses the notation and results derived in [11, 13, 18]. We will use this formalism to specifically address the problem of impedance matching between the chirped mirror coating and ambient medium. In Sect. 1, we give the exact description of multilayer interference coatings by exact coupled-mode equations [18]. Additionally, we extend this description by inclusion of the ambient medium. This is achieved with a similarity transformation of the coefficient matrix of the coupled-mode equations. The transformation matrix is the Fresnel matrix, which describes the refractive-index step between ambient medium and the first-layer material. We introduce the method of equivalent layers as an alternative exact description of a chirped mirror structure [19–21]. The design parameters of coupled-mode theory and the equivalent-layer design parameters are strongly related to each other [22]. As one result, the normalized equivalent (refractive) index (Herpin index) is the reciprocal of the characteristic impedance for the equivalent transmission-line model derived in [11]. With respect to the synthesis problem of a chirped mirror, this correspondence illustrates the equivalence of matching the impedance with matching the equivalent index. In Sect. 2 we discuss three examples, which differ in the degree of impedance matching achieved. In particular, we investigate matching to an ambient medium with a refractive index which is the geometric average of the high- and low-index material. Although this is a very intuitive and common choice (see, e.g., [23]), it does not provide perfect impedance matching as will become clear in the comparison with our final example. In Sect. 3 we present a practical example of a BASIC design. This design covers a bandwidth of 220 THz (610–1100 nm) for dispersion compensation in a Ti:sapphire laser. The design exhibits residual GDD oscillations of 5 fs^2 (peak-to-peak) or 2 fs^2 (rms), which is an order-of-magnitude improvement compared to previous design techniques. We compare dispersion and reflectance of manufactured coatings and designs. Experimental results are
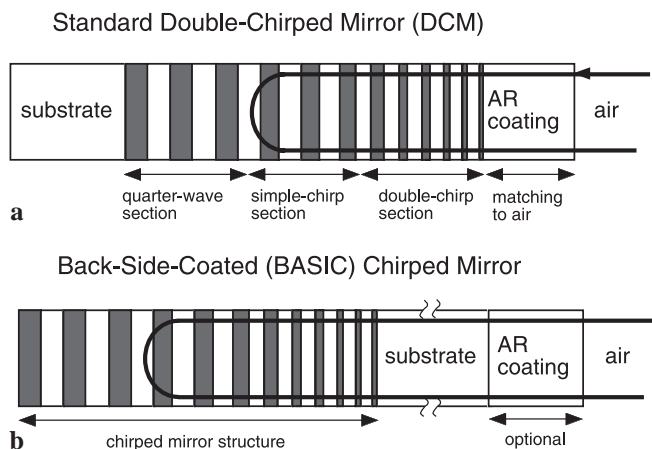
Standard Double-Chirped Mirror (DCM)

Back-Side-Coated (BASIC) Chirped Mirror

Fig. 1a,b. Schematic comparison of a standard double-chirped mirror **a** (DCM) and a back-side-coated **b** (BASIC) mirror. Both approaches employ the same functional components: a substrate, a chirped mirror structure and an anti-reflection coating (AR). In the conventional approach, AR and chirped mirror are coated on top of each other, whereas in case of the BASIC mirror the AR coating is optional and coated on the opposite side of the substrate. In **a**, the subdivision of the chirped coating into a double-chirp section, a simple-chirp section and an unchirped quarter-wave section is shown as described in [13]. The same approach can be employed for the chirped mirror structure of the BASIC mirror. In the following, examples of BASIC mirrors with simple-chirped coatings are also considered

described in Sect. 4. Using these mirrors in our laser, we generate pulses of 5.8-fs duration, which are then carefully characterized by spectral phase interferometry for direct electric-field reconstruction (SPIDER, [24, 25]). The deposition accuracy of ion-beam sputtering presently sets a limit to the dispersion oscillations of the manufactured coatings. In the near future, it is to be expected that improved in-situ monitoring schemes allow for an improved control of layer thickness to fully exploit the potential of the BASIC approach.

1 Exact coupled-mode theory and equivalent layers for the description of multilayer interference coatings

1.1 Exclusion of the ambient medium

A binary multilayer coating consists of a sequence of alternating layers with low and high refractive indices n_1 and n_2, respectively. For the theoretical considerations and examples in Sects. 1 and 2, we assume that the refractive indices are real quantities without any wavelength dependence. We compose the chirped Bragg structure by symmetrically defined unit cells according to Fig. 2a [11]. The values for the refractive indices may be chosen arbitrarily and $n_2 > n_1$ is not required. Figure 2b shows the resulting refractive-index profile for a sequence of three unit cells. Application of standard coupled-mode theory on such a multilayer stack neglects embedding of this structure into an ambient medium, e.g., air on the top and the substrate at the bottom side of the coating. Usually the influence of index discontinuities at both ends of the coating is taken into account after the coupled-mode differential equation system has been solved.

An exact description for chirped Bragg gratings is given by exact coupled-mode equations of the form [11]

$$\frac{d}{dm}\begin{pmatrix} A(m) \\ B(m) \end{pmatrix} = i \begin{pmatrix} -\delta(m) & -\kappa(m) \\ \kappa(m) & \delta(m) \end{pmatrix} \begin{pmatrix} A(m) \\ B(m) \end{pmatrix}. \tag{1}$$

In (1) A and B represent slowly varying normalized amplitudes of the right- and leftward propagating waves, respectively. The quasi-continuous variable m determines the position inside the mirror and counts the symmetric unit cells. By convention, m is a negative number. κ and δ denote the coupling and detuning coefficients, respectively. For non-uniform grating structures these coefficients are locally defined for each unit cell. As we have recently proven, a chirped mirror is exactly described by the coupled-mode equations (1), even for arbitrarily large refractive-index differences of the layer materials, provided the normalized coupling coefficient and detuning coefficient are properly defined. The exact coefficients can be written as [18, 22]

$$\kappa(m) = -\alpha(\varphi(m), \Delta\phi(m)) \frac{2r}{1-r^2}$$
$$\times \sin\left(\frac{1}{2}(\phi(m) + \Delta\phi(m))\right), \tag{2}$$

$$\delta(m) = -\alpha(\phi(m), \Delta\phi(m)) \frac{1}{1-r^2}$$
$$\times \left\{\sin(\phi(m)) + r^2 \sin(\Delta\phi(m))\right\}, \tag{3}$$
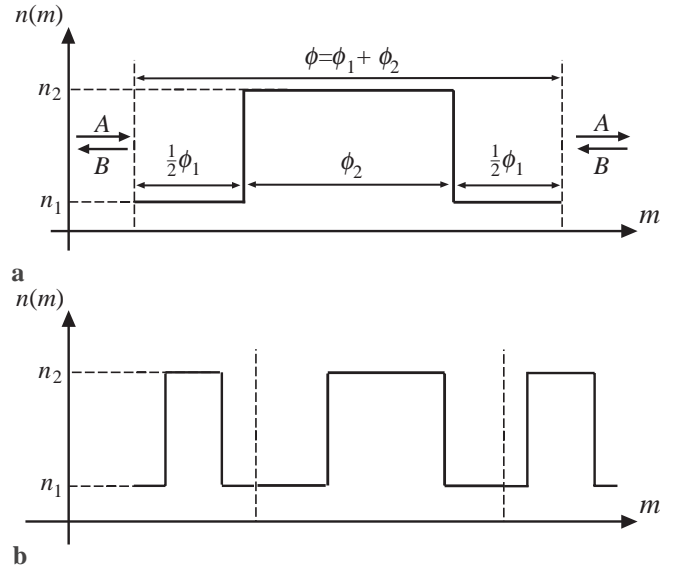

Fig. 2. a Refractive-index profile of the symmetrically defined unit cell. ϕ_i, $(i = 1, 2)$ denotes the phase shift in the different layers, yielding a total optical phase shift ϕ. The amplitude $A(m)$ refers to rightward-propagating waves, $B(m)$ to leftward-propagating waves. **b** Resulting index profile for a sequence of three unit cells

with

$$r = \frac{n_2 - n_1}{n_2 + n_1}, \tag{4}$$

$$\phi(m) = \phi_2(m) + \phi_1(m), \tag{5}$$

$$\Delta\phi(m) = \phi_2(m) - \phi_1(m), \tag{6}$$

$$\phi_1(m) = \frac{2\pi}{\lambda} n_1 d_{1,m}, \tag{7}$$

$$\phi_2(m) = \frac{2\pi}{\lambda} n_2 d_{2,m}. \tag{8}$$

In (2)−(8), r denotes the Fresnel reflectivity between the adjacent media 1 and 2, λ is the vacuum wavelength, and $d_{1/2,m}$ the physical thickness of layers 1 and 2 of the $|m|$th unit cell. $\phi_{1/2}(m)$ describes the optical phase shift in media 1 and 2, respectively. Thus $\phi(m)$ gives the total optical phase shift of the $|m|$th unit cell, and $\Delta\phi(m)$ is a measure of the duty cycle within this unit cell. The factor $\alpha = \gamma / \sin(\gamma)$ is defined by the exact propagation constant

$$\gamma = \sqrt{\delta^2 - \kappa^2} = \begin{cases} -i \ln\left(-F_R + \sqrt{F_R^2 - 1}\right); & F_R < -1 \\ \arctan\left(\frac{\sqrt{1-F_R^2}}{-F_R}\right); & -1 \leq F_R \leq 0 \\ -\arctan\left(\frac{\sqrt{1-F_R^2}}{F_R}\right) + \pi; & 0 < F_R \leq +1 \\ -i \ln\left(F_R - \sqrt{F_R^2 - 1}\right) + \pi; & F_R > +1 \end{cases} \tag{9}$$

with

$$F_R = \frac{1}{1-r^2}\left\{\cos(\phi) - r^2 \cos(\Delta\phi)\right\}, \tag{10}$$

using the definitions as given in [22]. The piecewise definition of γ allows for the distinction of different stop-band and passband regions. Complex values of γ (for $|F_R| > 1$) indicate the stop bands. In the first case ($F_R < -1$), the stop bands are centered at total phase shifts ϕ that are odd multiples of π. This includes the case of the fundamental Bragg wavelength at $\phi = \pi$. In the fourth case ($F_R > 1$) the stop bands are centered at even multiples of π.

In coupled-mode theory the coupling and detuning coefficients are design parameters, i.e., particular spectral response characteristics of a multilayer coating can be achieved by suitable choice of these parameters. For the design problem of a chirped mirror the concept of impedance matching plays an important role. As derived in [11], the exact coefficients (2) and (3) for the individual unit cells define a characteristic impedance Z according to

$$Z(m) = \sqrt{\frac{\delta(m) - \kappa(m)}{\delta(m) + \kappa(m)}} . \tag{11}$$

The oscillations observed in the dispersion properties of a chirped mirror are caused by an impedance mismatch in the front part of the mirror. The impedance can be matched by properly adjusting the coupling coefficient as a function of penetration depth [11]. Moreover, the GDD can be independently designed by suitable choice of the detuning coefficient with the chirp law [13]. It is important to note that κ, δ, and Z are not only functions of the considered unit cell $|m|$; they also depend on wavelength λ (see (7) and (8)).

Alternatively, multilayer coatings that are composed of symmetrically defined unit cells can be described by the method of equivalent layers [26, 27]. According to Herpin's theorem, every symmetrical combination of homogeneous layers is equivalent, at one arbitrary wavelength, to a single homogeneous layer [19]. This layer, called the equivalent layer, is characterized by its equivalent (refractive) index N_e (Herpin index) and its equivalent (phase) thickness Γ_e. At the design wavelength the substitution of multiple layers by an equivalent layer conserves the optical properties of the coating and is therefore exact. In the picture of equivalent layers, N_e and Γ_e act as design parameters, similar to the situation described above for the coupled-mode theory. Hence, we have an alternative formalism that exactly describes a multilayer coating by using a set of two design parameters.

As recently shown in [22], there is a formal equivalence between coupled-mode theory and the method of equivalent layers. Relations exist that directly link the coupled-mode parameters (κ, δ) with those describing the equivalent layer (N_e, Γ_e). For the three-layer combination shown in Fig. 2a, the following relations are valid:

$$\frac{N_e}{n_1} = \frac{1}{Z} = \sqrt{\frac{\delta + \kappa}{\delta - \kappa}}$$
$$= \sqrt{\frac{\sin(\phi) + r^2 \sin(\Delta\phi) + 2r \sin[(\phi + \Delta\phi)/2]}{\sin(\phi) + r^2 \sin(\Delta\phi) - 2r \sin[(\phi + \Delta\phi)/2]}} , \tag{12}$$

$$\cos(\Gamma_e) = \cos(\gamma + \pi) = F_R$$
$$= \frac{1}{1 - r^2} \left\{ \cos(\phi) - r^2 \cos(\Delta\phi) \right\} , \tag{13}$$

where (2), (3), and (9)−(11) have been used. Thus, the normalized equivalent index is the reciprocal of the characteristic

impedance Z^{-1}, and the equivalent thickness is essentially given by the exact propagation constant, γ. Inversion of (13) results in a multi-valued solution for Γ_e. We take the solution derived in [22], which is compatible with the definition given in [20]. In contrast to the constant indices n_1 and n_2, the equivalent index shows a strong wavelength dependence. Moreover, for wavelengths in the stop-band regime the equivalent-layer parameters become complex. It follows from (12) that the impedance-matching problem of a chirped mirror translates into the problem of matching the equivalent index, as will be discussed in detail in Sect. 2. Additionally, finding an appropriate chirp law by adjusting the propagation constant γ via the detuning coefficient δ is equivalent to a proper choice of the equivalent thickness along the chirped mirror structure according to (13).

1.2 Inclusion of the ambient medium

Now we incorporate the index discontinuity at the ambient medium/coating interface into our coupled-mode description. We define the refractive-index profile of the unit cell as shown in Fig. 3a, i.e., we include the step of the refractive index from medium 1, n_1, to the refractive index of the ambient medium, n_a, at both ends of the unit cell. Figure 3b shows the refractive-index profile of a sequence of three unit cells. Inside the mirror structure, the downward steps and subsequent upward steps cancel each other. At the ends of the structure, however, an index step from material 1 to the respective ambient medium remains. This symmetric description of the unit
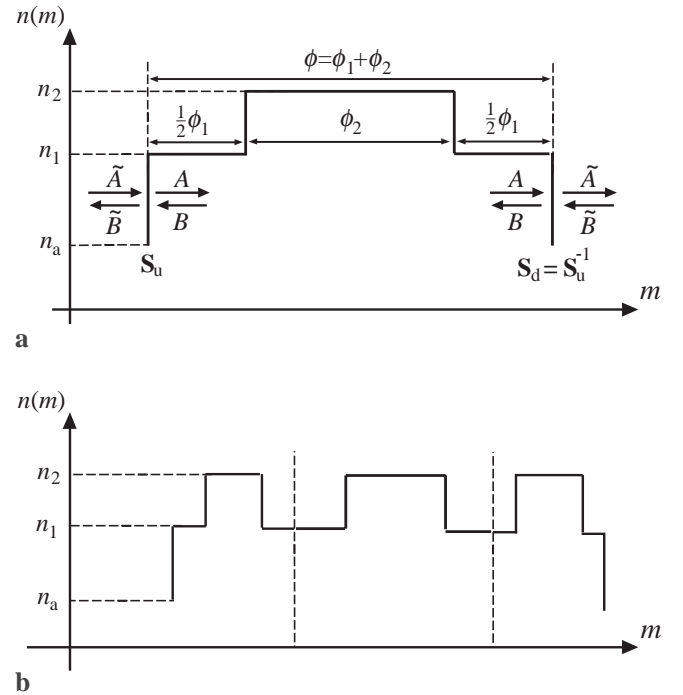

Fig. 3. a Modified refractive-index profile of the unit cell defined for the inclusion of the ambient medium. Transfer matrices S_d and S_u convert amplitudes A and B inside the layer stack into amplitudes $\tilde{A}$ and $\tilde{B}$ in the ambient medium as shown. Note that symmetric inclusion may be assumed without loss of generality in the case of a high-reflectivity coating, as effectively no light propagates through the layer structure. **b** Resulting index profile for a sequence of three unit cells. Note that upward and downward index steps cancel except for the ends of the coating structure

cells presupposes that the refractive indices of both ambient media (e.g. substrate and air) are equal, which is generally not the case. However, for highly reflecting mirror coatings, as considered in this paper, this is irrelevant as almost no light passes through the coating.

Mathematically, the terminal discontinuity of the refractive index is described by Fresnel transfer matrices S_u and S_d for the upward and downward steps, respectively. These transfer matrices transform the amplitudes A and B into new amplitudes $\tilde{A}$ and $\tilde{B}$ (see Fig. 3a). We write

$$\begin{pmatrix} \tilde{A}(m) \\ \tilde{B}(m) \end{pmatrix} = S_u \begin{pmatrix} A(m) \\ B(m) \end{pmatrix} \Leftrightarrow \begin{pmatrix} A(m) \\ B(m) \end{pmatrix} = S_d \begin{pmatrix} \tilde{A}(m) \\ \tilde{B}(m) \end{pmatrix}, \qquad (14)$$

with the Fresnel matrices [18]

$$S_u = \frac{1}{2\sqrt{n_a n_1}} \begin{pmatrix} n_a + n_1 & n_a - n_1 \\ n_a - n_1 & n_a + n_1 \end{pmatrix} = S_d^{-1}, \qquad (15)$$

$$S_d = \frac{1}{2\sqrt{n_a n_1}} \begin{pmatrix} n_a + n_1 & -(n_a - n_1) \\ -(n_a - n_1) & n_a + n_1 \end{pmatrix} = S_u^{-1}. \qquad (16)$$

Using the transformation (14), we obtain the following new coupled-mode equations for the transformed amplitudes

$$\frac{d}{dm} \begin{pmatrix} \tilde{A}(m) \\ \tilde{B}(m) \end{pmatrix} = i \begin{pmatrix} -\tilde{\delta}(m) & -\tilde{\kappa}(m) \\ \tilde{\kappa}(m) & \tilde{\delta}(m) \end{pmatrix} \begin{pmatrix} \tilde{A}(m) \\ \tilde{B}(m) \end{pmatrix}, \qquad (17)$$

where the transformed coefficient matrix is given by

$$\begin{pmatrix} -\tilde{\delta}(m) & -\tilde{\kappa}(m) \\ \tilde{\kappa}(m) & \tilde{\delta}(m) \end{pmatrix} = S_u \begin{pmatrix} -\delta(m) & -\kappa(m) \\ \kappa(m) & \delta(m) \end{pmatrix} S_u^{-1}. \qquad (18)$$

Thus, the new coefficients are obtained from the original ones by a similarity transformation. Evaluating (18) yields the following explicit expressions for the transformed exact coupling and detuning coefficients

$$\tilde{\kappa} = c_1 \kappa + c_2 \delta, \qquad (19)$$

$$\tilde{\delta} = c_1 \delta + c_2 \kappa, \qquad (20)$$

with

$$c_1 = \frac{1}{2} \left(\frac{n_1}{n_a} + \frac{n_a}{n_1} \right), \qquad (21)$$

and

$$c_2 = \frac{1}{2} \left(\frac{n_1}{n_a} - \frac{n_a}{n_1} \right). \qquad (22)$$

We can immediately see that the transformed coupling and detuning coefficients reduce to the original coefficients (2) and (3) in the case of an ambient medium with a refractive index equal to the index of medium 1, i.e., $n_a = n_1$. Table 1 summarizes examples of transformation coefficients (21) and (22) that will be discussed in Sect. 2. The coefficient c_1 is always close to unity, whereas the value of c_2 strongly varies. c_2 is a direct measure of the index discontinuity between the ambient medium and medium 1 and essentially describes the difference between transformed and original coefficients.

Table 1. Values of the transformation coefficients c_1 and c_2 for the design studies of Sect. 2

	c_1	c_2
A. No impedance matching	1.08	0.42
B. Partial impedance matching	1.03	-0.26
C. Perfect impedance matching	1.00	0.00

Using (11) and (19)−(22) the transformed impedance follows as

$$\tilde{Z}(m) = \sqrt{\frac{\tilde{\delta}(m) - \tilde{\kappa}(m)}{\tilde{\delta}(m) + \tilde{\kappa}(m)}} = \frac{n_a}{n_1} Z(m) = \frac{n_a}{N_e}. \qquad (23)$$

Finally, we note that the equivalent-layer parameters are invariant under the transformation (14), i.e., $\tilde{N}_e = N_e$ and $\tilde{\Gamma}_e = \Gamma_e$.

2 Impedance matching to the ambient medium

Comparing the coupled-mode equations (1) with (17) we see that both equations are exactly of the same form. Hence, all equations and conclusions derived in [11–13] still hold, provided the transformed coefficients (19)−(22) are used instead of (2) and (3). The conditions for the suppression of dispersion oscillations

$$Z(m = 0) = 1 \quad \forall \delta \Rightarrow \kappa(m = 0) = 0, \qquad (24)$$

$$\tilde{Z}'(m = 0) = 0 \quad \forall \delta \Rightarrow \kappa'(m = 0) = 0. \qquad (25)$$

provide perfect impedance matching of the chirped mirror structure to an ambient medium with the same refractive index as medium 1 (see [11]). The prime in (25) denotes the derivative with respect to m. Condition (24) states that, according to (12), the equivalent index must equal the index of medium 1 at the mirror front. Moreover, for perfect matching, condition (25) requires that the equivalent index be ramped up or down as slowly and smoothly as possible.

The same conditions also hold for the transformed coupled-mode parameters, i.e.,

$$\tilde{Z}(m = 0) = 1 \quad \forall \tilde{\delta} \Rightarrow \tilde{\kappa}(m = 0) = 0, \qquad (26)$$

$$\tilde{Z}'(m = 0) = 0 \quad \forall \tilde{\delta} \Rightarrow \tilde{\kappa}'(m = 0) = 0. \qquad (27)$$

According to (23), these impedance-matching conditions are equivalent to matching of the equivalent index of the unit cell to the refractive index of the ambient medium. Generally, for an arbitrary ambient medium, finding a broadband solution satisfying these conditions is very difficult because of the strong wavelength dependence of the equivalent index.

In Sects. 2.1−2.3, we investigate matching condition (26) for three ambient media with different refractive indices n_a. Without loss of generality, we restrict ourselves to the investigation of (26). If this condition is satisfied, condition (27) can be always fulfilled by a sufficiently slow change of the design parameters. We find large differences in the quality of the design, depending on the degree of impedance matching

achieved and indicated by the magnitude of dispersion oscillations. In the following examples, we choose the refractive indices $n_1 = 1.5$ and $n_2 = 2.5$ for the layer materials, leading to $r = 0.25$. These values are chosen as they are close to the indices of SiO_2 and TiO_2, commonly used as dielectric coating materials.

2.1 No impedance matching

In the first example, we assume that the ambient medium is air, i.e., $n_a = 1.0$. In terms of dispersion oscillations we want to discuss this as the worst possible case. We refrain from any attempts to improve impedance matching at the interface to air and consider a plain simple-chirped mirror structure. A simple-chirped mirror refers to a multilayer structure with a gradually increasing Bragg wavelength but a constant 50% duty cycle, i.e., $\phi_1(m) = \phi_2(m) \forall m$.

Figure 4 shows the response characteristics of a simple-chirped mirror. In this example, the Bragg wavelength is chirped over the initial 20 unit cells and then kept constant for another five unit cells to increase the reflectance for long wavelengths. The reflectance is very high over a broad wavelength range and covers most of the Ti:sapphire gain spectrum. However, the group delay (GD) shows extremely large oscillations, similar to a Gires–Tournois interferometer (GTI, [28]), with a peak-to-peak amplitude on the order of 100 fs, which makes such a mirror useless for ultra short-pulse generation.

Obviously, the simple-chirped mirror structure does not provide any impedance matching. To further investigate this, we explore the transformed coupled-mode design parameters $(\tilde{\kappa}, \tilde{\delta})$ and the equivalent-layer parameters (N_e, Γ_e) as two-dimensional functions of the unit cell and wavelength, depicted as contour plots. In these plots the x-axis gives the unit cell and the y-axis gives the incident wavelength. It is assumed that the light is incident from the right. In Fig. 5a the contour lines of the transformed coupling coefficient (19) are almost horizontal lines with values far
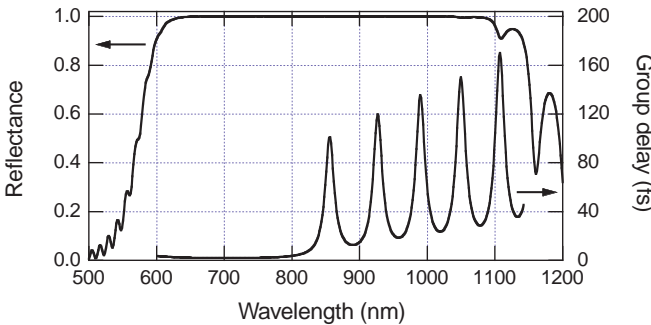
Fig. 4. Calculated amplitude *(left axis)* and phase *(right axis)* properties of a standard front-coated simple-chirped mirror as a function of wavelength. Shown are the reflectance and the group delay upon reflection, respectively. In this example the Bragg wavenumber is linearly decreased over the first 20 unit cells from the maximum value $k_B^{max} = 2\pi/(650\,\text{nm})$ to the minimum value $k_B^{min} = 2\pi/(950\,\text{nm})$ according to $k_B(m) = k_B^{max} - (|m|-1)\left(k_B^{max} - k_B^{min}\right)/19$. For the last five unit cells the Bragg wavenumber is kept constant at its minimum value k_B^{min}. Air has been assumed as the ambient medium. The simple-chirped mirror provides a broad high-reflectance range, but exhibits strong dispersion oscillations over most of this range
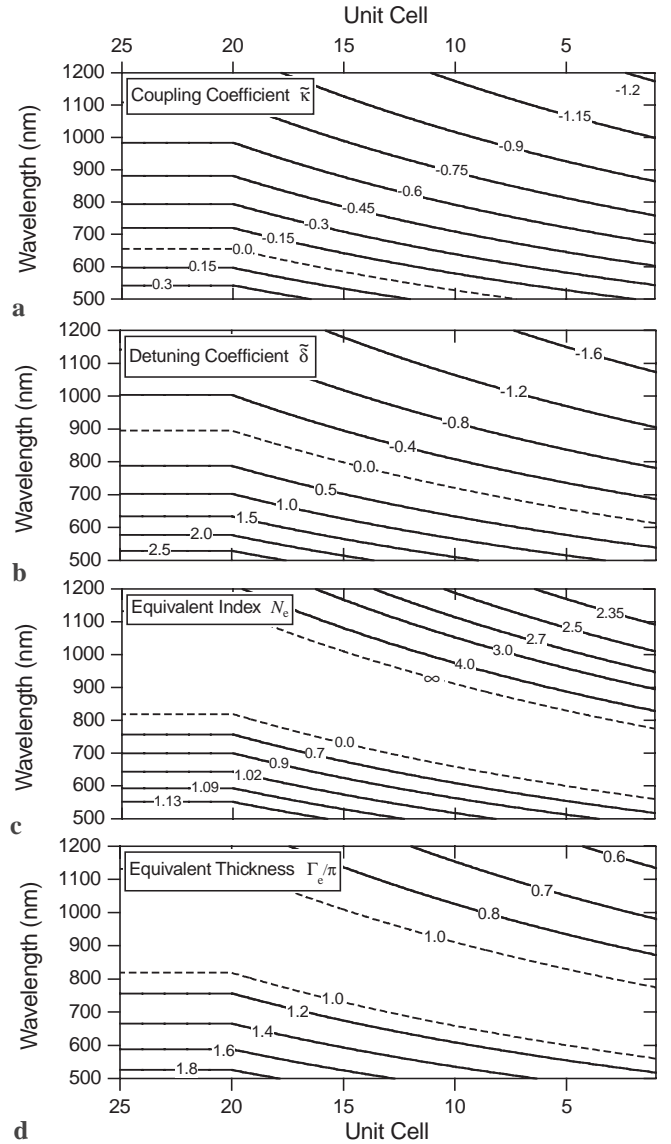
Fig. 5. a Contour plots of the transformed coupling coefficient $\tilde{\kappa}$, **b** the detuning coefficient $\tilde{\delta}$, **c** the equivalent index N_e, **d** and the equivalent thickness Γ_e (in units of π) of the simple-chirped mirror of Fig. 4 as functions of unit cell $|m|$ and wavelength

from zero at the coating surface. Condition (26) is not fulfilled for any given wavelength in the high-reflectance region. In fact, the transformed coupling coefficient in Fig. 5 is even farther from being matched to zero than the original coupling coefficient. The original coupling coefficient is always negative and approximately constant due to the simple-chirped mirror structure ($\kappa \approx -2r = -0.5$, [22]). According to (19), matching can only be achieved by positive values of $c_2\delta$. For wavelengths above 650 nm, however, this is not fulfilled at the coating surface because of the negative detuning coefficient δ. Consequently, absolutely no impedance matching is achieved in this simple-chirped structure.

Figure 5b shows the contour lines of the transformed detuning coefficient. These contour lines are nearly linear functions over the range of chirped Bragg wavenumbers. According to (20), the transformed detuning coefficient essentially

follows the original detuning coefficient with an offset of $c_2\kappa \approx -0.2$. The qualitative behavior of the detuning coefficient is not changed by the transformation. The zero contour line of the original detuning coefficient indicates the Bragg condition, i.e., the dependence of Bragg wavelength on penetration depth or chirp law. Compared to the original detuning coefficient, the zero contour line of the transformed detuning coefficient is shifted by $\approx 50\,\mathrm{nm}$ to shorter wavelengths (dashed line). This plot clearly illustrates the approximately linear increase of the GD with wavelength (negative GDD).

This scenario can be also interpreted in the picture of equivalent layers. According to Sect. 1, impedance matching requires that the equivalent index at the mirror front equals the refractive index of the ambient medium ($n_a = 1.0$). However, Fig. 5c shows that the equivalent index is extremely far from being matched to unity at the mirror front, illustrating the large impedance mismatch. The broad area surrounded by contour lines with the values zero and infinity marks the stop-band region, where the equivalent index becomes complex. For this region the unit cells represent a potential barrier with an exponential behavior of the electromagnetic field. In the passband regions outside the evanescent region, the equivalent index is real and the unit cells are transparent for the light. With respect to the quantum-mechanical scattering problem as introduced in [11], the upper line ($N_e = \infty$) corresponds to right turning points and the lower line $N_e = 0$ to left turning points of the corresponding classical motion.

Figure 5d shows that, for a fixed wavelength, the equivalent thickness of the unit cells monotonically increases with penetration depth, illustrating the chirp of the Bragg wavelength along the mirror structure. As mentioned above, custom-tailored dispersion properties can be designed by a proper control of the equivalent thickness. For passband regions the equivalent thickness of unit cell $|m|$ approximately corresponds to the total optical phase shift (5) evaluated at wavelength λ [22]. Similarly to Fig. 5c, the evanescent region is surrounded on both sides by the dashed unity contour line (given in units of π).

2.2 Partial impedance matching

In the second example we again consider the case of a simple-chirped mirror, but now we search for the refractive index of the ambient medium with best possible impedance matching without additional matching layers (e.g., an AR coating). It might be suspected that best matching is achieved if the index of the ambient medium is the geometric average of the indices of media 1 and 2. Structures matched to the geometric average of the refractive indices have been used before as a starting design for chirped mirrors (see, e.g., [23]). We will exemplify, however, that this method does not yet lead to the optimum solution for the impedance-matching problem considered and only provides partial impedance matching.

For a simple-chirped mirror with $\Delta\phi(m) = 0\,\forall m$, using (12) and (23) the impedance-matching condition (26) is rewritten as

$$\tilde{Z}(m) = \frac{n_a}{n_1}\sqrt{\frac{\sin(\phi) - 2r\sin(\phi/2)}{\sin(\phi) + 2r\sin(\phi/2)}} \overset{!}{=} 1 .\qquad(28)$$

From this the ambient refractive index can be resolved as

$$n_a = n_1\sqrt{\frac{\cos(\phi/2) + r}{\cos(\phi/2) - r}} .\qquad(29)$$

The right-hand side of (29) is the equivalent index as a function of the phase variable ϕ. Impedance matching requires that (29) be fulfilled over a broad wavelength range, i.e., the equivalent index should equal the index of the ambient medium n_a independent of the total phase shift ϕ. The refractive index of the ambient medium is a real quantity. This requires $\phi < 2\arccos(|r|)$ as a necessary condition if we restrict ourselves to phase shifts $\phi \leq \pi$. The equivalent index is approximately constant only for sufficiently small phase shifts ϕ close to zero, see Fig. 6. In particular, this figure clearly illustrates the strong wavelength dependence of the equivalent index, as mentioned in Sect. 1. In the limit $\phi \to 0(\lambda \to \infty)$ we get the long-known result [21]:

$$n_a = n_1\sqrt{\frac{1 + r}{1 - r}} = \sqrt{n_1 n_2} .\qquad(30)$$

This is exactly the geometric average refractive index of both layer materials. The limit $\phi \to 0$ appears to be in contradiction to the assumption of quarter-wave layers, where $\phi \approx \pi$ for wavelengths near the Bragg wavelength. In this relevant case, the impedance-matching condition practically requires us to start chirping at Bragg wavelengths much smaller than the minimum design wavelength of the coating. In other words, the impedance-matching condition $\phi \to 0$ is only fulfilled for wavelengths much larger than the Bragg wavelength of the unit cell considered.

Let us consider the example of a simple-chirped mirror structure in Figs. 7 and 8. Unlike in the previous example
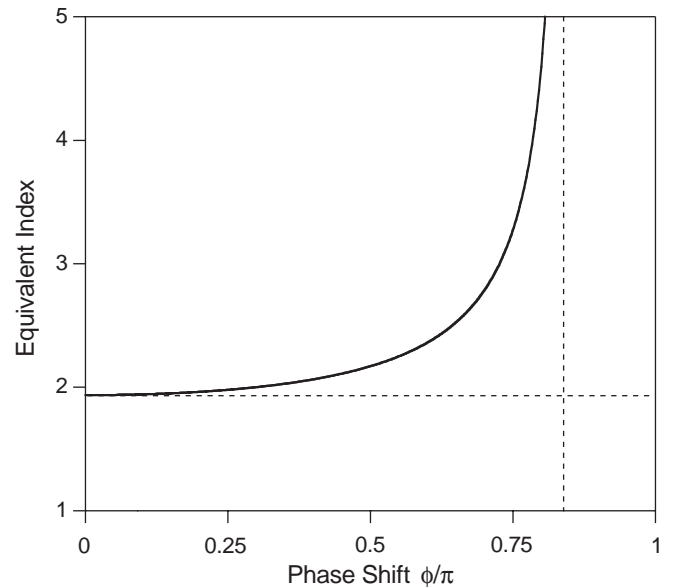

Fig. 6. Equivalent index as a function of phase shift as given by (29). As in the other examples, $n_1 = 1.5$, $n_2 = 2.5$ has been assumed. For small values of ϕ, the equivalent index approaches the geometric average of n_1 and n_2, i.e., $n_a = 1.94$. The equivalent index diverges for $\phi \to 2\arccos(|r|)$ and is complex-valued for the fundamental stop-band region at Bragg resonance $\phi_B = \pi$
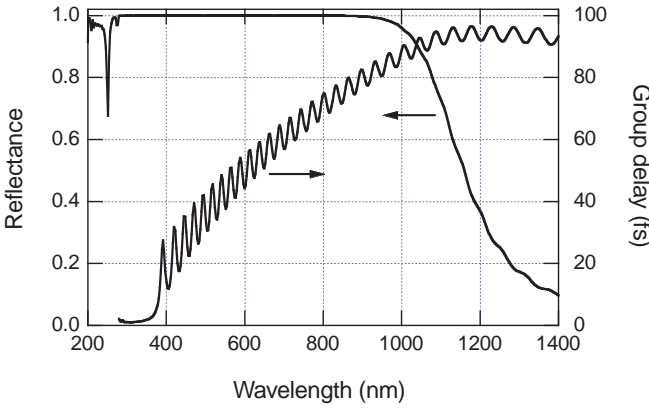
Fig. 7. Calculated reflectance *(left axis)* and group delay *(right axis)* of a back-side-coated simple-chirped mirror as a function of wavelength. The Bragg wavenumber is linearly decreased over 50 unit cells from $k_B^{max} = 2\pi/(300\,\text{nm})$ to $k_B^{min} = 2\pi/(1000\,\text{nm})$. A material with the geometric average of the coating materials ($n_a \approx 1.94$) has been assumed as the ambient medium. The back-side-coated simple-chirped mirror provides partial impedance matching, as indicated by the reduced dispersion oscillations over most of this range

(Figs. 4 and 5) we now assume an ambient medium with an index equal to the geometrical average of the two layer materials. For a coating providing dispersion compensation from 600 nm to 1000 nm, we start chirping the Bragg wavelength at 300 nm. The high-reflectance range of the coating is extremely wide as shown in Fig. 7, but most of this range lies well out of the band with phase properties that might be useful for dispersion compensation. The GD oscillations with a peak-to-peak amplitude of about 10 fs are considerably reduced compared to Fig. 4. The dispersion oscillations decrease with an increasing wavelength but never reduce to a negligible value. The curve is far from being smooth and such oscillations are not tolerable for an ultra-short-pulse laser source. Reducing the number of layers and increasing the initial Bragg wavelength of the design further deteriorates the phase properties of the coating. On the other hand, dispersion properties at 800 nm may be improved by starting to chirp at even lower Bragg wavelengths < 300 nm. In any case, only a small part of the spectrum is covered, providing high reflectance and decent dispersion properties simultaneously.

The contour plots shown in Fig. 8 further illustrate the partially achieved impedance matching. Still, the contour lines at the mirror front are essentially horizontal lines similar to the contour lines shown in Fig. 5. In contrast, matching condition (26) is now partially fulfilled, as indicated by the contour plots for the transformed coupling coefficient and for the equivalent index (see Fig. 8a and c). These contour plots confirm that matching is improved at longer wavelengths. With increasing wavelength the coupling coefficient approximates zero, Fig. 8a, and the equivalent index in Fig. 8c approaches n_a given by (30).

In conclusion, assuming quarter-wave layers and an ambient medium with a geometric average of the indices of media 1 and 2 provides a partial reduction of dispersion oscillations. The quality of impedance matching, however, is directly related to the excess bandwidth, with excellent reflectance but poor dispersion properties. Therefore, this design approach makes very uneconomic use of the available
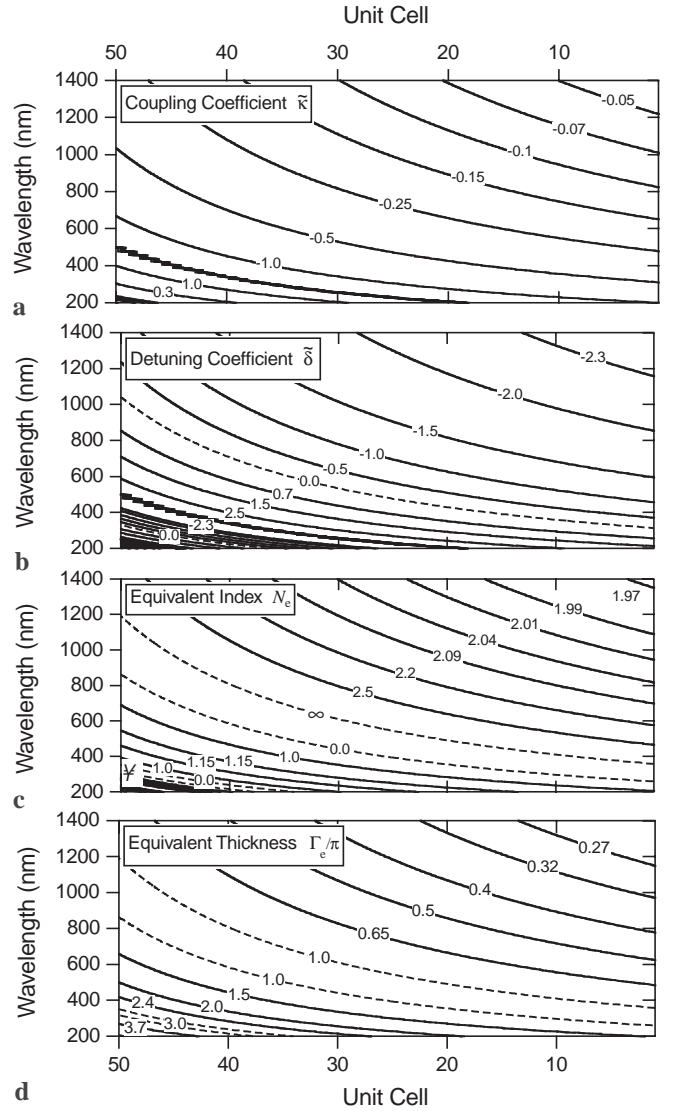

Fig. 8. a Contour plots of the transformed coupling coefficient $\tilde{\kappa}$, **b** the detuning coefficient $\tilde{\delta}$, **c** the equivalent index N_e, **d** and the equivalent thickness Γ_e (in units of π) of the back-side-coated simple-chirped mirror of Fig. 7 as functions of unit cell $|m|$ and wavelength

number of layers, which renders it impracticable for many applications.

2.3 Perfect impedance matching

In the final example, we assume that the ambient medium has the same refractive index as medium 1, i.e., $n_a = n_1 = 1.5$. As mentioned in Sect. 1, this reduces the transformed coupled-mode parameters to the original ones and matching condition (26) reduces to the old matching condition (24). According to [11], the DCM design technique now allows for perfect impedance matching. This means using very thin layers of material 2 for the initial unit cells in the mirror structure, i.e., $n_2 d_{2,m} \ll \lambda_B(m)/4$, and then slowly ramping up the duty cycle of the coating until 50% is reached, i.e., $n_2 d_{2,m} = \lambda_B(m)/4$. With the DCM technique, the coupling coefficient vanishes according to (2) and (4–8), and the impedance equals unity according to (11). Other than in a standard DCM,

however, no broadband AR coating is required to match the index to the ambient medium.

Figure 9 shows reflectance and GD of a DCM consisting of 25 unit cells. The Bragg wavenumber is linearly chirped over the first 20 unit cells and then kept constant for the remaining five unit cells in the same way as in Sect. 2.1. In Sect. 2.3, however, a material with an index identical to the low-index layer material has been assumed as the ambient medium. Also, we independently chirp the thickness of the material 2 over the first 12 unit cells (double-chirping). The very smooth dispersion over the entire high-reflectance range in Fig. 9 clearly illustrates the resulting effect of impedance matching. This comes at the expense of a slight reduction of the high-reflectance bandwidth on the short-wavelength side, as a comparison of Figs. 4 and 9 reveals [11].

In Fig. 10a the (transformed) coupling coefficient of the DCM is plotted. At the beginning of the mirror structure, the contour lines are almost vertically oriented. Each individual unit cell provides an almost constant coupling coefficient for any given wavelength. The coupling coefficient vanishes at the beginning, indicating excellent broadband impedance matching. The absolute value of the coupling coefficient increases along the grating structure until it reaches its maximum value. The behavior of the (transformed) detuning coefficient shown in Fig. 10b generally resembles the first example shown in Fig. 5b. In contrast, however, the detuning values of Fig. 10b are shifted towards larger values. The zero contour line pinpoints Bragg resonance, yielding the chirp law [13].

The high degree of impedance matching achieved is also clearly illustrated by the contour plot of the equivalent index. For the passband region at the mirror front, the contour lines are essentially vertical lines with a value close to 1.5 over a broad wavelength range. This demonstrates again the almost perfect matching to the refractive index of the ambient medium. The equivalent thickness plotted in Fig. 10d shows the same qualitative behavior as the equivalent thickness in the first example (see Fig. 5d). However, one deviation be-
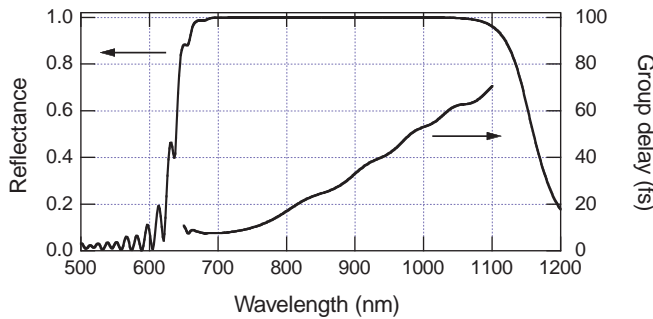

Fig. 10. a Contour plots of the coupling coefficient $\tilde{\kappa}$, **b** the detuning coefficient $\tilde{\delta}$, **c** the equivalent index N_e, **d** and the equivalent thickness Γ_e (in units of π) of the BASIC double-chirped mirror in Fig. 9 as functions of unit cell $|m|$ and wavelength. Note that in **a** and **b** transformed and original values for the coupling coefficient and the detuning coefficient are identical

tween the equivalent-layer parameters of Figs. 5 and 10 is very obvious. For short wavelengths at the mirror front the dashed contour lines, which surround the stop-band region, are narrower, indicating the reduction of the high-reflection bandwidth for short wavelengths (compare Figs. 4 and 9).

3 BASIC mirror design

3.1 Substrate properties

The theoretical findings of Sects. 1 and 2 now offer a convenient method to avoid dispersion oscillations of chirped mirrors by proper design. Choosing an index of refraction of the ambient medium identical to the index of one of the coating materials, perfect impedance matching at this interface is achieved by double-chirping of the chirped mirror structure. Practically, this means inversion of the layer sequence

Fig. 9. Calculated reflectance *(left axis)* and group delay *(right axis)* of a BASIC double-chirped mirror as a function of wavelength. In this example the Bragg wavenumber is linearly decreased over the first 20 unit cells from the maximum value $k_B^{max} = 2\pi/(650 \text{ nm})$ to the minimum value $k_B^{min} = 2\pi/(950 \text{ nm})$ according to $k_B(m) = k_B^{max} - (|m|-1)(k_B^{max} - k_B^{min})/19$. For the last five unit cells the Bragg wavenumber is kept constant at its minimum value k_B^{min}. The thickness of the material 2 is varied with penetration depth according to $d_{2,m} = \pi/(2k_B(12)n_2)(|m|/12)^{1.2}$ over the first 12 unit cells (double-chirp section in Fig. 1). A material with an index equal to the low-index material of the coating has been assumed as the ambient medium ($n_a = n_1 = 1.5$). The BASIC double-chirped mirror provides a broad high-reflectance range and smooth dispersion characteristics, simultaneously
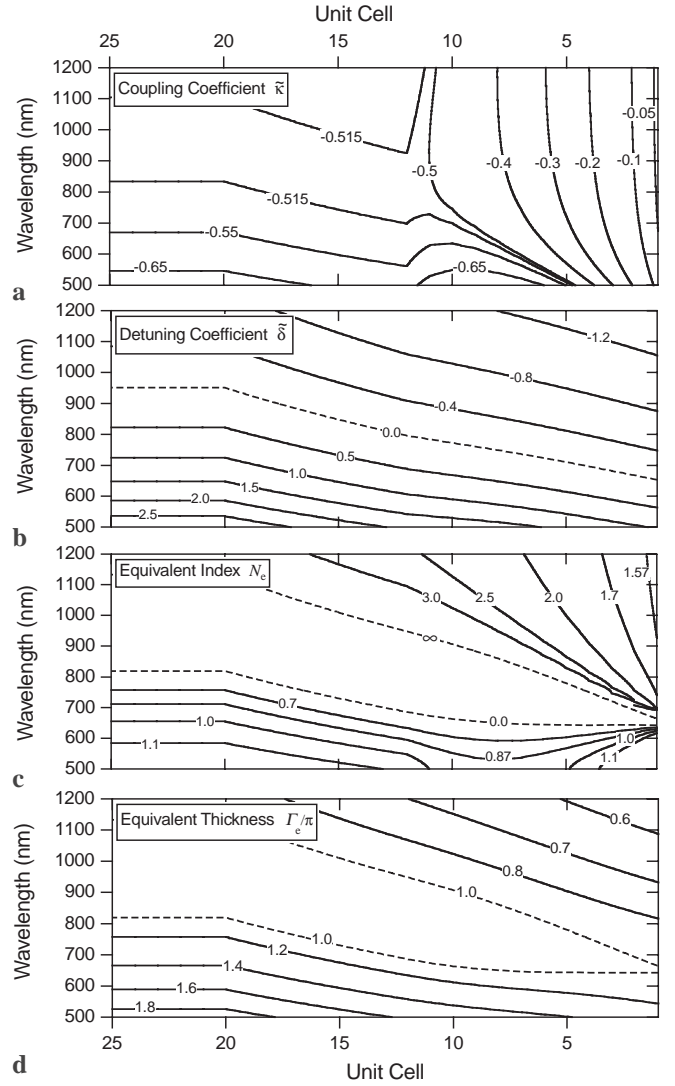
and coating the layers on the back side of a substrate. Consequently, the light beam passes through the substrate before reflection by the chirped mirror coating. Therefore, we name this method back-side-coated (BASIC) chirped mirrors.

It might appear difficult to choose a substrate material with exactly matching index because the refractive index of sputtered or evaporated materials may significantly deviate from the refractive index of bulk materials. A refractive index $n_{SiO_2} \approx 1.49$, e.g., for sputtered silica compares to a bulk value $n_{FS} \approx 1.45$ at 800 nm. Such an index discontinuity at the interface between coating and substrate, however, merely causes a reflection of 2×10^{-4} at normal incidence. A further reduction is achieved by suitable choice of an optical glass with a refractive index closer to sputtered SiO_2 (e.g., BK7 with $n_{BK7} \approx 1.51$ at 800 nm). In any case, the problem of residual mismatch between substrate and coating index is far less stringent than the problem of matching to air. A residual mismatch of the order discussed above is easily resolved by numerical optimization of the layer sequence.

One might argue that the BASIC approach only transfers the impedance-matching problem to the opposite interface of the substrate. In fact, if plane-parallel substrates were used, interference with the reflection from the interface to air gives rise to pronounced satellite pulses. With the high reflection from the back and the partial Fresnel reflection from the top, such a mirror would form a GTI, causing a strong spectral variation of the mirror phase. However, these detrimental interference effects are suitably suppressed by a geometrical mismatch of the two surfaces. This can be achieved by making the two surfaces non-parallel and therefore non-interfering, i.e., by wedging or by choosing different centers of curvature for the two surfaces. Residual interference is calculated from the overlap of the reflections in the far field. For typical applications in a laser cavity with beam divergences of a few mrad, wedge angles on the order of one degree readily reduce interference to a negligible amount for a plane mirror. To replace the concave focusing mirrors in a typical laser cavity, thin plano-convex lens substrates may be used to diminish interference effects.

The geometrical mismatch of the substrate surfaces allows for suppression of detrimental interference effects by any given degree, but the power losses caused by the Fresnel reflection at the top surface appear prohibitive for use inside a laser cavity. Of course, an AR coating on the front surface of the BASIC mirror readily reduces this problem. Additionally, an AR coating further suppresses dispersion oscillations caused by a small residual overlap of the beams in the far field and allows for a smaller geometrical mismatch of the two surfaces. Hence, even though it is not strictly required, the AR coating also improves the dispersion properties of the BASIC mirror.

The total dispersion of a BASIC mirror is given by the dispersion of the chirped mirror structure plus twice the dispersion of substrate and AR coating upon transmission. Typical chirped mirror coatings for use in Ti:sapphire lasers allow for the compensation of material dispersion equivalent to a path length of about 2-mm fused silica per bounce [29]. Therefore, it is desirable to use substrates of a few 100-μm thickness to permit the generation of a net negative GDD with a BASIC mirror. On the other hand, however, multilayer coatings of 60 or more layers are known to generate tensile or compressive stress on the substrate, causing a deformation of extremely thin substrates. In our experiments we found a substrate thickness of about 0.5 mm a viable compromise between surface deformation and tolerable material path.

3.2 Optimized design for ultra-short-pulse Ti:sapphire lasers

For BASIC chirped mirrors, one has to design two independent coatings, an AR coating for the top surface and the chirped mirror coating for the back surface. We use an 18-layer AR coating and a 60-layer BASIC coating for the coverage of the gain bandwidth of Ti:sapphire (650–1100 nm) with both high net reflectance and smooth dispersion properties. The AR coating is designed using commercial software [30]. Figure 11a depicts the residual reflectivity of about 10^{-3} for the given wavelength range. Note that this coating also provides high transmission for the pump wavelengths 488 and 514 nm (argon-ion laser). Figure 11b shows the resulting GDD of the BASIC AR coating upon transmission with nearly negligible dispersion over the entire gain bandwidth of Ti:sapphire.

The 60-layer chirped mirror coating on the back surface is designed according to [13] and is subsequently computer-optimized with a local gradient algorithm [31]. The design goals are a high reflectance and a smooth GDD over the 450-nm wavelength range of the AR coating. Additionally, the mirror has to be highly transparent for the pump laser. The mirror is designed for p-polarized light with an incidence angle of 5° in air. This corresponds to an incidence angle of $\approx 3.44°$ in the fused silica substrate. Figure 12 depicts the spectral response characteristics of the resulting BASIC DCM structure, calculated for fused silica as the incident
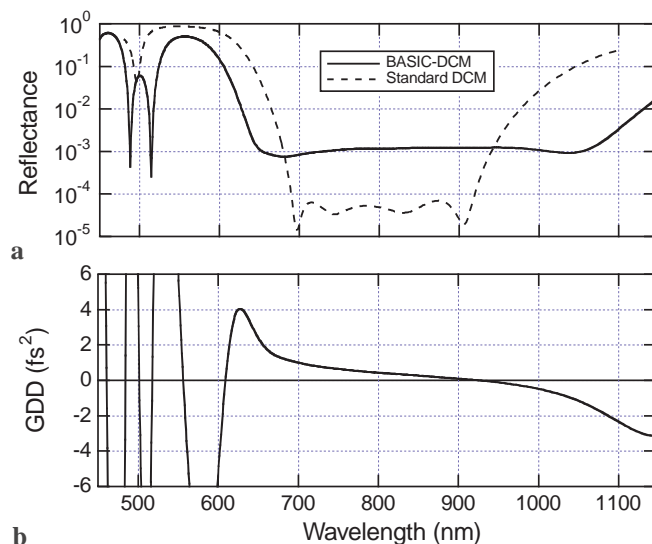

Fig. 11. a Reflectance of two AR coatings with different bandwidth. The dashed line shows a 14-layer AR coating that provides about 240-nm bandwidth with less than 10^{-4} reflectance as used in standard DCMs [11]. The solid line refers to an ultra-broadband coating (18 layers) with more than 400-nm bandwidth and about 10^{-3} residual reflectance as used on the front surface of the BASIC chirped mirror. As the AR coating is passed twice per bounce, the effective losses amount to double the residual reflectance of the coating. The ultra-broadband coating also provides high transmission at the pump wavelengths 488 and 514 nm. **b** Group delay dispersion of the ultra-broadband AR coating upon transmission
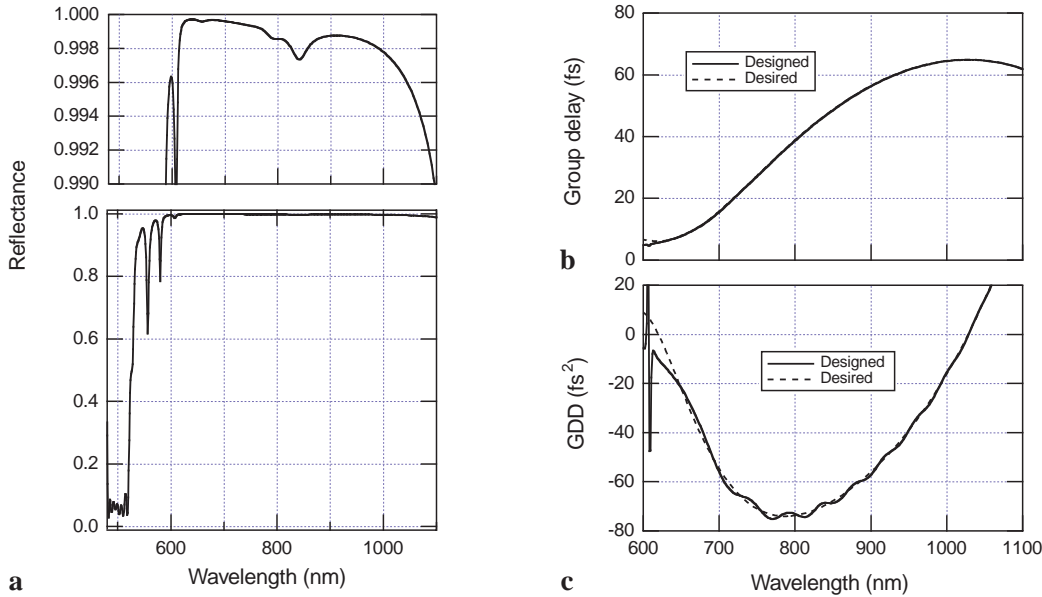
Fig. 12. a Calculated reflectance of a BASIC double-chirped mirror structure. The structure is designed for use in an ultra-short-pulse Ti:sapphire laser. In a computer optimization process, a highly transmissive window for the pump laser is introduced. Measured refractive-index data for the coating materials are used. In these calculations, the influence of AR coating and substrate on spectral properties is not considered. The reference plane is chosen in the substrate close to the coating, isolating the effect of the DCM coating. The reflectance is plotted on two different scales to show the high reflectance in the 620- to 1050-nm range and the transmissive region at 500 nm. **b** Designed *(solid line)* and desired *(dashed line)* group delay of the BASIC double-chirped mirror structure upon reflection. Note that both curves practically coincide except for the short-wavelength end of the range shown. **c** Designed *(solid line)* and desired *(dashed line)* GDD of the BASIC double-chirped mirror structure upon reflection

medium. The chirped mirror structure provides a 99.8% reflectance from 610–1000 nm (190 THz bandwidth). Accounting for the additional 0.2% losses due to the double pass through the AR coating, this results in a net reflectivity of 99.6% over the same 400-nm bandwidth. The wide reflectance range favorably matches the unprecedented bandwidth of extremely smooth dispersion of 220 THz.

3.3 Comparison to standard DCMs

Comparison of the structure of a BASIC mirror and a standard DCM readily reveals three identical functional sections but in a different order: a substrate, a chirped mirror structure, and an AR coating (Fig. 1). In the case of the BASIC mirror, however, the two coating sections are non-interfering, separated by the substrate in between. The non-interference of the two coating sections decouples their design, and imperfections of the AR sections do not spoil the dispersion properties of the mirror. Figure 11a illustrates this by comparing the reflectance of the AR coating used in the BASIC design approach with similar 14-layer coatings used in the design of previous standard DCMs [11]. Due to the high sensitivity of the DCM dispersion towards residual reflection from the AR section, the residual reflectivity has to be kept at 10^{-4} or below, which limits the bandwidth of such a coating to about 250 nm at 800-nm center wavelength. Given the layer materials and the 450-nm bandwidth of this design, the residual reflectivity generally saturates at about 10^{-3} with only marginal improvement from an increased number of layers [32]. Consequently, any attempt to further increase the bandwidth of standard DCM coatings causes a dramatic increase of dispersion oscillations.

In contrast, the BASIC approach tolerates a residual reflectance of 10^{-3} for use inside a Ti:sapphire laser, and this can be immediately traded for 200 nm of extra bandwidth. The BASIC design technique is mainly limited by the achievable net reflectivity rather than by the magnitude of dispersion oscillations as in conventional DCM designs. The insensi-
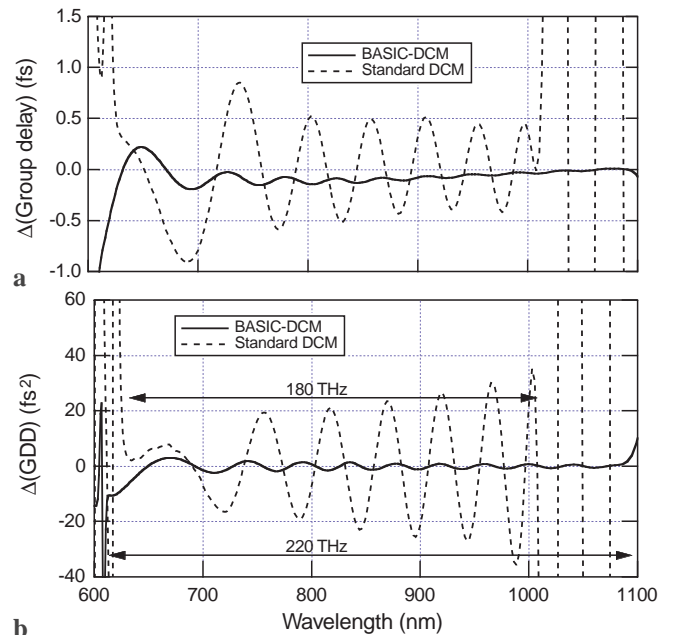

Fig. 13a,b. Dispersion oscillations of BASIC double-chirped mirrors *(solid line)* and standard DCMs *(dashed line)*. Data from Fig. 12 and [1] have been used for this comparison. Shown are the differences between desired and designed values of **a** group delay and **b** GDD

tivity towards dispersion oscillations is illustrated in Fig. 13, comparing the dispersion properties of a BASIC DCM and a conventional DCM. Both coatings shown use 60 layers, of which 14 are used in the AR section of the standard DCM. This example clearly shows that the BASIC design approach reduces dispersion oscillations to a peak-to-peak value of 5 fs^2 (2 fs^2 rms), whereas the standard DCM of significantly less bandwidth exhibits peak-to-peak oscillations of 50 fs^2 (15 fs^2 rms).

Some additional advantages of the BASIC approach should be pointed out. With the weak remaining impedance-matching problem, computer optimization of the coating structure is less demanding than in the conventional DCM design approach. Using the same number of layers in a BASIC mirror, a wider wavelength range can be covered because no layers have to be sacrificed for impedance matching to air. Finally, the AR coating of a BASIC mirror may be grown independently, using materials with higher index contrast to further increase the net reflectance.

The design in Fig. 12 may serve as an illustration of how to achieve optimum performance given the bandwidth and other constraints of a mode-locked Ti:sapphire laser. Giving up the highly transmissive region around 500 nm used for pumping the laser allows for an additional reduction of dispersion oscillations in the design. A further extension of the dispersion-compensation bandwidth, e.g., for the compression of white-light supercontinua, is possible by allowing for a reduced net reflectance or using more layers. For applications outside a laser cavity, slightly increased losses typically pose no problem. In principle, support of single-cycle spectra with BASIC chirped mirrors is feasible in external compression schemes.

4 Experimental results

4.1 Back-side-coated chirped mirrors

The design presented in Sect. 3 was grown using high-precision ion-beam sputtering [33]. Active control of layer deposition in the few-Angstrom range [34] is indispensable because of the high sensitivity of the GDD to deposition errors [12, 23]. We used 0.45-mm-center-thickness plano-convex lens substrates as a replacement for the 10-cm-radius concave focusing mirrors previously used in our laser. The convex side of the lens substrates has a radius of curvature of 150 mm (focal length $f = R/2n \approx 5$ cm) and is coated with the BASIC chirped mirror structure. The AR coating is applied to the plane surface. During polishing, the thin lens substrates are optically contacted to plane carrier substrates. With the support of the carrier substrates, surface deformations of the substrates can be kept below $\lambda/5$ (peak-to-valley values over 1-cm diameter) in the manufacturing process. For the coating process, the substrates are removed from the carrier. With the chirped mirror coating applied, the thin lens substrates are finally cemented into mating concave 10-mm-thick carrier substrates, similar to the construction of an achromatic lens. Cementing to a carrier substrate prevents mechanical stress to the thin mirrors and also protects the chirped mirror coatings from environmental influences. The internal stress of the coating is decreased by the reduced substrate curvature. Since the BASIC DCM is buried behind

the lens, the front surface can be cleaned with no danger of mechanical damage to the chirped mirror coating. The final structure consisting of the thin BASIC DCM lens and the thick glass support forms a mechanically rugged slab with two flat surfaces. The back side of the thick supporting glass substrate can be additionally AR-coated to improve transmission of the pump light.

We use white-light interferometry to characterize the dispersion of the manufactured mirrors. Figure 14a shows the measured GDD of a BASIC chirped mirror in comparison with the target GDD of the design. Note that these curves now include twice the GDD of a 0.45-mm substrate and twice the GDD of the AR coating upon transmission. We
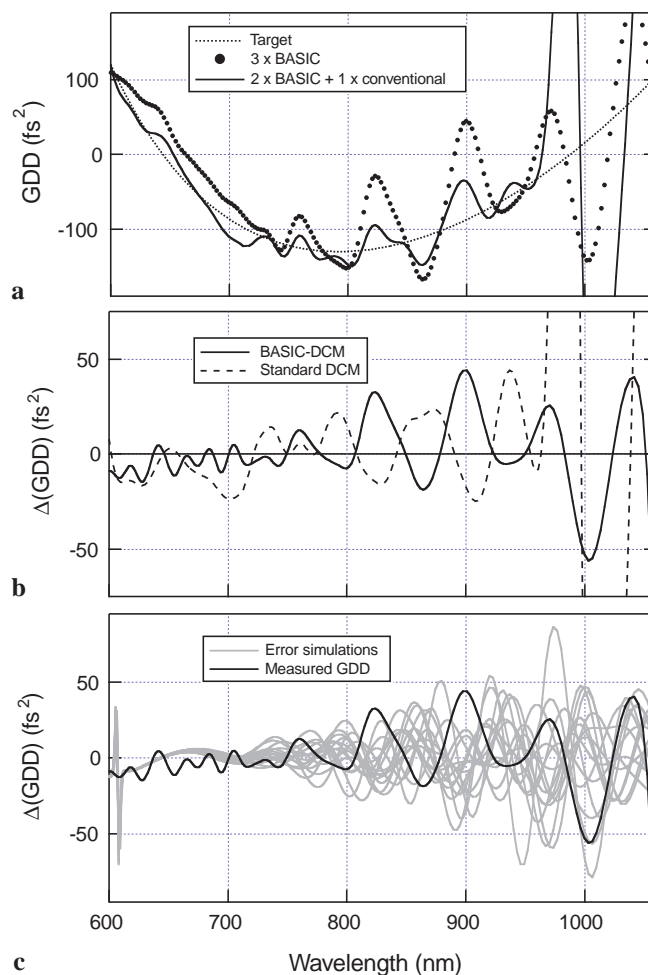

Fig. 14. a Desired round-trip GDD (single pass through fused silica prism sequence with 50-cm apex separation and 2.3 mm of Ti:sapphire) used as a target function for the mirror design *(dotted line)*. The measured GDD of the BASIC chirped mirror is shown as *dots*. Note the net positive dispersion of the BASIC mirror at 900 nm. In comparison with Figs. 12 and 13, dispersion of the AR coating (Fig. 11b) and the substrate with a measured thickness of 0.45 mm are now included. **b** The differences between designed and manufactured GDD are shown (BASIC chirped mirror, *solid line*; standard DCM [1], *dashed line*). The standard DCM exhibits similar dispersion oscillations, which are, however, shifted such that they partially cancel out dispersion oscillations of the BASIC mirror. A combination of one standard DCM and two BASIC mirrors yields smooth dispersion compensation from 650 nm to 950 nm, shown as the *solid line* in **a**. The magnitude of the dispersion oscillations of the BASIC mirror coating agrees with numerical simulations, indicating a 2-Å (rms) layer-deposition accuracy (**c**)

find an excellent agreement between designed and manufactured dispersion with small residual dispersion oscillations up to a wavelength of about 800 nm. For longer wavelengths, which penetrate deeper into the mirror structure, deposition errors become noticeable and the GDD oscillation amplitude exceeds the designed value. But still, up to a wavelength of about 950 nm the resulting dispersion oscillations are of the same magnitude as in previously grown DCMs, which are shown for comparison in Fig. 14b. Compared to standard DCMs, the BASIC mirrors again exhibit much smaller dispersion oscillations at longer wavelengths up to 1050 nm. In summary, the manufactured BASIC mirrors exhibit a similar magnitude of dispersion oscillations but cover a 100-nm-wider bandwidth.

Our simulations (Fig. 14c) indicate an rms layer growth accuracy of ≈ 2 Å, for both the standard DCMs and the BASIC mirrors manufactured. Although this is an excellent value, it is still necessary to combine mirrors to compensate for manufacturing defects. A further reduction of manufacturing errors to about ≈ 1 Å per layer appears necessary in order to use BASIC mirrors of similar bandwidth directly without compensation for manufacturing errors and to fully exploit their potential in an oscillator.

4.2 Ultra-short-pulse Ti:sapphire laser

In initial attempts to use three BASIC mirrors in a Ti:sapphire laser, we did not succeed to push the mode-locked spectrum beyond the positive net dispersion region at 900 nm. Previously, we solved similar problems with standard DCMs by combining mirrors from one coating run under different angles of incidence [1]. Increasing the angle generally allows shifting the dispersion oscillations of a particular mirror towards shorter wavelengths. As we did not have a flat BASIC mirror available as would be required for that purpose, we used a combination of two BASIC chirped mirrors and one standard DCM to reduce the dispersion oscillations. The standard DCM is identical to the mirrors used in [1]. All mirrors are now used at near-normal incidence. The net dispersion of the mirror combination is shown in Fig. 14a. Note how dispersion oscillations of the individual mirrors cancel out for the wavelength range from 780 nm to 970 nm (Fig. 14b). Together, two BASICs and one standard DCM yield a relatively smooth net dispersion, ranging from 650 nm to 970 nm with maximum dispersion oscillations of 80 fs^2 (peak-to-peak value, for a single pass through the cavity). The described mirror combination is used in a Kerr-lens mode-locked Ti:sapphire laser otherwise similar to [1]. Compared to the set-up described earlier, two of the focusing mirrors inside the cavity are replaced by BASIC chirped mirrors and the flat folding mirror is taken out. To balance the average negative GDD in both resonator arms, the standard DCM with stronger negative GDD is placed in the resonator arm with the semiconductor saturable-absorber mirror (SESAM). The fused silica prism pair (50-cm apex separation) introduces negative GDD in the other resonator arm that contains the OC mirror. Compared to [1] a slightly shifted output coupling mirror design is used to optimize spectral shaping. Standard DCMs are also used for the external compression scheme. The pulses are fully characterized by spectral phase interferometry for direct electric-field reconstruction (SPIDER, [24, 25]). Spectral intensity and phase
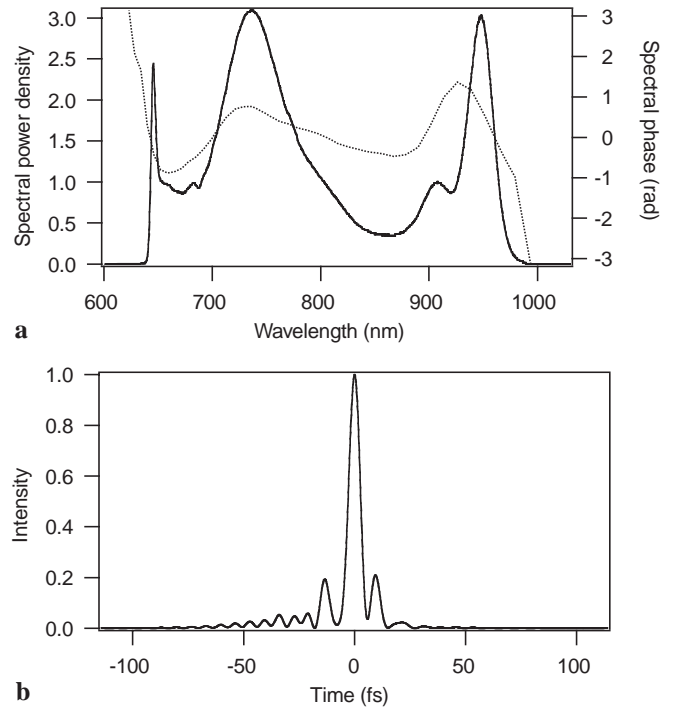

Fig. 15a,b. SPIDER measurement of pulses from a Kerr-lens mode-locked Ti:sapphire laser employing two BASIC chirped mirrors (see Figs. 12–14). **a** Measured spectral power density *(solid line)* and phase *(dashed line)*. Assuming a flat phase, the transform-limited duration of the pulse is 5.6 fs. The corresponding intracavity spectrum exhibits a transform limit of 6.7 fs. **b** Reconstructed temporal profile of the pulse with a pulse duration (full width at half maximum) of 5.8 fs

and the resulting pulse profile in the time domain are shown in Fig. 15. We measure a pulse duration of 5.8 fs. Our measurements indicate that the pulse duration is very close to the bandwidth limit of 5.6 fs and significantly lower than the intracavity transform limit of 6.7 fs. Taking into account that there is still one conventional DCM in the cavity, these results agree favorably with the 5.9 fs achieved with only conventional DCMs. The results achieved with the BASIC mirrors are within 3% of the bandwidth limit, resulting in a nearly transform-limited pulse. In a slightly different configuration, we also obtained very clean pulses of about 7-fs duration. The latter pulses have strongly reduced satellites with less than 5% of the main pulse and exhibit a nearly bell-shaped spectrum. This configuration made use of a broadband OC mirror of 5.5% transmission, surrendering spectral shaping upon output coupling [15]. In summary, the results obtained with the BASIC mirrors clearly demonstrate the potential of our new mirror design approach. Our experiments show that given the current state of the art of layer-deposition accuracy and substrate manufacturing the BASIC design approach can be successfully used in a sub-6-fs laser. With a similar dispersion-oscillation amplitude, the bandwidth of the BASIC mirrors is clearly enhanced compared to earlier designs.

5 Conclusions

We have reviewed the matching problems of chirped mirror structures to the ambient medium. The analytical findings and numerical investigations show that the double-chirped mirror

522

technique provides an optimum solution to the impedance-matching problem if an ambient medium with index identical to one of the layer materials is chosen. The resulting design approach of BASIC chirped mirrors allows for ultra-broadband dispersion compensation with virtually no dispersion oscillations. A comparison with standard DCMs clearly demonstrates the superiority of the BASIC design approach. Over a bandwidth of 220 THz (610–1100 nm), GDD oscillations of $2\,\mathrm{fs}^2$ (rms) can be achieved, which presents an order-of-magnitude improvement compared to earlier designs of less bandwidth. We use BASIC chirped mirrors inside a Kerr-lens mode-locked Ti:sapphire laser to generate near-bandwidth-limited 5.8-fs pulses. Despite the clearly extended bandwidth of the manufactured mirrors, deposition errors of BASIC chirped mirrors are still a limiting factor for the further reduction of dispersion oscillations. With expected improvements of fabrication accuracy, the BASIC technique will allow for chirped mirror structures with negligibly small dispersion oscillations. Besides use inside an oscillator, BASIC mirrors appear very attractive for external white-light continuum compression schemes [6, 7] and optical parametric amplifiers [8], which can greatly benefit from the extended bandwidth. BASIC mirrors promise an improvement of dispersion control for octave-exceeding pulse spectra, which is a very important prerequisite to push pulse durations further into the single-cycle regime.

References

1. D.H. Sutter, G. Steinmeyer, L. Gallmann, N. Matuschek, F. Morier-Genoud, U. Keller, V. Scheuer, G. Angelow, T. Tschudi: Opt. Lett. **24**, 631 (1999)
2. U. Morgner, F.X. Kärtner, S.H. Cho, Y. Chen, H.A. Haus, J.G. Fujimoto, E.P. Ippen, V. Scheuer, G. Angelow, T. Tschudi: Opt. Lett. **24**, 411 (1999); Opt. Lett. **24**, 920 (1999)
3. R.L. Fork, C.H.B. Cruz, P.C. Becker, C.V. Shank: Opt. Lett. **12**, 483 (1987)
4. J. Zhou, G. Taft, C.-P. Huang, M.M. Murnane, H.C. Kapteyn, I.P. Christov: Opt. Lett. **19**, 1149 (1994)
5. R. Szipöcs, K. Ferencz, C. Spielmann, F. Krausz: Opt. Lett. **19**, 201 (1994)
6. A. Baltuska, M.S. Pshenichnikov, D.A. Wiersma: Opt. Lett. **23**, 1474 (1998)
7. M. Nisoli, S. De Silvestri, O. Svelto, R. Szipöcs, K. Ferenz, C. Spielmann, S. Sartania, F. Krausz: Opt. Lett. **22**, 522 (1997)
8. A. Shirakawa, I. Sakane, M. Takasaka, T. Kobayashi: Appl. Phys. Lett. **74**, 2268 (1999)
9. G. Steinmeyer, D.H. Sutter, L. Gallmann, N. Matuschek, U. Keller: Science **286**, 1507 (1999)
10. L. Xu, G. Tempea, A. Poppe, M. Lenzner, C. Spielmann, F. Krausz, A. Stingl, K. Ferencz: Appl. Phys. B **65**, 151 (1997)
11. N. Matuschek, F.X. Kärtner, U. Keller: IEEE J. Sel. Top. Quantum Electron. **4**, 197 (1998)
12. F.X. Kärtner, N. Matuschek, T. Schibli, U. Keller, H.A. Haus, C. Heine, R. Morf, V. Scheuer, M. Tilsch, T. Tschudi: Opt. Lett. **22**, 831 (1997)
13. N. Matuschek, F.X. Kärtner, U. Keller: IEEE J. Quantum Electron. **QE-35**, 129 (1999)
14. I.D. Jung, F.X. Kärtner, N. Matuschek, D.H. Sutter, F. Morier-Genoud, G. Zhang, U. Keller, V. Scheuer, M. Tilsch, T. Tschudi: Opt. Lett. **22**, 1009 (1997)
15. D.H. Sutter, L. Gallmann, N. Matuschek, F. Morier-Genoud, V. Scheuer, G. Angelow, T. Tschudi, G. Steinmeyer, U. Keller: Appl. Phys. B **70**, S5 (2000)
16. V. Laude, P. Tournois: In Conference on Lasers and Electro-Optics (CLEO '99), CTuR4, 1999
17. N. Matuschek, F.X. Kärtner, U. Keller: In Conference on Lasers and Electro-Optics (CLEO '98), CThC6, 1998
18. N. Matuschek, F.X. Kärtner, U. Keller: IEEE J. Quantum Electron. **QE-33**, 295 (1997)
19. A. Herpin: Compt. Rend. **225**, 182 (1947)
20. L.I. Epstein: J. Opt. Soc. Am. **42**, 807 (1952)
21. A. Thelen: J. Opt. Soc. Am. **56**, 1533 (1966)
22. N. Matuschek, G. Steinmeyer, U. Keller: Appl. Opt. **39**, 1626 (2000)
23. R. Szipöcs, A. Kohazi-Kis: Appl. Phys. B **65**, 115 (1997)
24. C. Iaconis, I.A. Walmsley: IEEE J. Quantum Electron. **QE-35**, 501 (1999)
25. L. Gallmann, D.H. Sutter, N. Matuschek, G. Steinmeyer, U. Keller, C. Iaconis, I.A. Walmsley: Opt. Lett. **24**, 1314 (1999)
26. H.A. Macleod: *Thin-Film Optical Filters* (Adam Hilger, Bristol 1985)
27. A. Thelen: *Design of Optical Interference Coatings* (McGraw-Hill, New York 1989)
28. F. Gires, P. Tournois: C. R. Acad. Sci. Paris **258**, 6112 (1964)
29. D.H. Sutter, I.D. Jung, F.X. Kärtner, N. Matuschek, F. Morier-Genoud, V. Scheuer, M. Tilsch, T. Tschudi, U. Keller: IEEE J. Sel. Top. Quantum Electron. **4**, 169 (1998)
30. A.V. Tikhonravov, M.K. Trubetskov: SPIE Conf. Proc. **2253**, 10 (1994)
31. W.H. Press, S.V. Teukolsky, W.T. Vetterling, B.P. Flannery: Numerical Recipes in Fortran (Cambridge University Press 1994)
32. J.A. Dobrowolski, A.V. Tikhonravov, M.K. Trubetskov, B.T. Sullivan, P.G. Verly: Appl. Opt. **35**, 644 (1996)
33. V. Scheuer, M. Tilsch, T. Tschudi: SPIE Conf. Proc. **2253**, 445 (1994)
34. M. Tilsch, V. Scheuer, J. Staub, T. Tschudi: SPIE Conf. Proc. **2253**, 414 (1994)